Electronic Supplementary Material (ESI) for Journal of Materials Chemistry A.
This journal is © The Royal Society of Chemistry 2021

Supporting Information

Coacervation-driven instant paintable underwater adhesives with tunable optical and electrochromic properties

Qiongyao Peng,[a] Jingsi Chen,[a] Tao Wang,[a] Lu Gong,[a] Xuwen Peng,[a] Meng Wu,[a] Yuhao Ma,[b] Feiyi Wu,[a] Diling Yang,[a] Hao Zhang,[a] and Hongbo Zeng[a]*

[a]*Department of Chemical and Materials Engineering, University of Alberta, Edmonton, Alberta T6G 1H9, Canada.*

[b] *Department of Biomedical Engineering, University of Alberta, Edmonton, Alberta T6G 2V2, Canada*

**Corresponding Authors. E-mail: hongbo.zeng@ualberta.ca (H. Zeng); Fax: +1-780-492-2881; Tel: +1-780-492-1044*

Supporting Information Includes:

Table S1. Summary of the reported wet/underwater adhesives.

Figure S1-S12

Figure S1. Corresponding pictures of the phase diagram between SiW and P123 with various concentrations. (Left: upon mixing of the two aqueous solutions; Right: after centrifugation)

Figure S2. Viscosities of SiW40-P123-10, SiW40-P123-15, SiW40-P123-20 coacervates with shear rate ranging from 0.1 to 100/s.

Figure S3. FTIR spectra of P123, SiW and freeze-dried SiW40-P123-10 coacervate.

Figure S4. Variations of viscosity versus temperature for SiW40-P123-10 coacervate, SiW40-PEG8000-10 coacervate and 10 wt% P123 aqueous solution.

Figure S5. Pictures for the formation of SiW40-P123-10 coacervate and the corresponding supernatant prepared with SiW solution at pH=1.14 (left) and the mixture of 40 wt% SiW (pH= 1.75) and 10 wt% P123 aqueous solutions (right).

Figure S6. Calculation of volumes of the SiW-P123 coacervate phases and corresponding supernatants as well as concentration of SiW in the SiW-P123 coacervate phases.

Figure S7. Shear storage modulus, shear loss modulus and viscosity of SiW40-P123-10 coacervate and SiW40-PEG8000-10 coacervate.

Figure S8. Shear loss modulus G'' and shear storage modulus G' of SiW40-P123-10, SiW40-P123-15, SiW40-P123-20, SiW40-F68-10, SiW40-F68-15, SiW40-F68-20 coacervates.

Figure S9. (a-b) Microtubes and micropores on the wood surface observed under an optical microscope coupled with AFM. (c)AFM image of the rough wood surface. (d-g) SiW40-P123-10 coacervate could spread on the wood surface.

Figure S10. The change of transmittance at 550 nm of the SiW40-P123-10 coacervate with temperature ranging from 21 ℃ to 60 ℃.

Figure S11. Shear loss modulus and viscosity of P123 aqueous solution at temperatures of 20 ℃ and 60 ℃.

Figure S12. CNTs-loaded SiW40-P123-10 coacervate and corresponding schematic intermolecular interactions.

Movie S1-S8

Movie S1: Coalescence process of coacervate droplets.

Movie S2: Underwater paintability of SiW40-P123-10 coacervate and its resistance to flush of running water immediately after being painted underwater.

Movie S3: The SiW40-P123-10 coacervate could facilely bind different materials such as wood, coin, stone, and glass slide as well as a plastic substrate underwater.

Movie S4a: The SiW40-P123-10 coacervate instantly and firmly adhered two weights together underwater and easily support a mass of 100 g.

Movie S4b: The SiW40-P123-10 coacervate could instantly bind two porcine skins underwater which could endure repeatable movement and swing.

Movie S5: Thermo-responsive optical properties of the SiW40-P123-10 coacervate where the coacervate painted on a glass slide was successively immersed in 60 ℃ water bath and 0 ℃ ice-water bath for several cycles.

Movie S6: The SiW40-P123-10 coacervate adhesive could be directly painted on different substrates and display excellent resistance to mechanical deformation such as stretching and bending. Meanwhile, CNTs-encapsulated P123 micelles could be further coacervated into the SiW40-P123-10 coacervate phase.

Movie S7: A self-powered electrochromic device built up by connecting a coacervate-painted indium tin oxide (ITO) glass slide with an Al foil through salt bridge and metal wire. Once the circuit was completed, the coacervate coating instantaneously changed from white to deep blue, and then the blue color could be bleached with the disconnection of the circuit and addition of H_2O_2 (30 wt%).

Movie S8: Two ITO-coated glass slides were bonded together with the coacervate and connected to an external voltage provided by an electrochemical workstation. When a reduction potential of -0.25 V was applied, the coacervate immediately turned to be deep blue.

Table S1. Summary of the reported wet/underwater adhesives.

Components of Wet/underwater adhesives	Adhesive type	Fabrication methods	Molecular interactions	Effective time	Adhesive strength (kPa)	Stimuli-responsiveness	Ref.
Silicotungstic acid and P123 micelles	Coacervate	Simple mixing	Hydrogen bonding interactions	Instant or 10 s	479.6, underwater	Thermo-tunable optical property and electrochromism	**This work**
Silicotungstic acid and PEG	Coacervate	Simple mixing	Hydrogen bonding interaction	60 s	98.2, wet	n/a	1
Tannic acid and 4-arm PEG-NH_2	Coacervate	Simple mixing	Hydrogen bonding interaction	60 s	180, wet	n/a	2
Tannic acid and polyamidoamine-epichlorohydrin	Coacervate	Simple mixing	Electrostatic and hydrogen bonding interactions	24 h	458.2, underwater	n/a	3
lignosulfonate and apolyamidoamine-epichlorohydrin	Coacervate	Simple mixing	Electrostatic interaction	Instant	122.3	n/a	4
Tannic acid and poly(vinyl alcohol)	Coacervate	Simple mixing	Hydrogen bonding interaction	30 s	~80, underwater	n/a	5
Silicotungstic acid and histidine	Coacervate	pH adjustment and simple mixing	Electrostatic interaction	4 h	436.7, wet	n/a	6
Nonionic polyester	Coacervate	Complex polymer synthesis	Covalent bond, hydrophobic and hydrogen bonding interactions	20 min	~80, underwater	n/a	7
Poly(allylamine), pyrophosphate/ tripolyphosphate	Coacervate	Simple mixing	Electrostatic interaction	3 h	~440, underwater	pH- and ionic strength-responsiveness	8
Pentaerythritol tetraacrylate, dopamine, PEGDA	Hyperbranched Polymer-based coacervate	Polymer synthesis	Covalent bond and hydrophobic interaction	12 h	390	n/a	9
Cationic and aromatic monomers	Hydrogel	Free-radical polymerization	Covalent bond and cation-π interactions	5 s	~70, underwater	n/a	10
Cationic and aromatic monomers	Hydrogel	Free-radical polymerization	Covalent bond and cation-π interactions	10 s	180, underwater	n/a	11
Tannic acid and silk fibroin	Hydrogel	Simple mixing	Electrostatic and hydrogen bonding interactions	20 min	134.1, wet with water or blood	n/a	12
N-acryloyl 2-glycine and hydroxyapatite	Organic-inorganic Hydrogel	One-pot radical polymerization	Electrostatic and hydrogen bonding interactions	Instant	140, wet	n/a	13
Polyacrylic acid and amorphous calcium carbonate	Organic-inorganic Hydrogel	Mixing and rinsing	Chelation between Ca^{2+} and COO^-	24 h	~250, underwater	n/a	14
Hydrophilic and hydrophobic monomers	Organo-hydrogel	Complex polymer synthesis	Hydrogen bonding and hydrophobic interactions	30 min	13.2, underwater or in organic solvent	n/a	15
$H_6P_2W_{18}O_{62}$ and 3-(2-naphthyl)-l-alanine	Coating	Complex synthesis and 60 ℃ heat treatment	Electrostatic interaction	15 min	14.67, underwater	Electrochromism	16
pDOPA-AD-MEA and pNIPAM-CD	Surface with thermo-responsive coating	Free-radical polymerization and deposition of adhesive coating	Host-guest molecular interaction	Instant	~4, underwater	Thermo-induced underwater adhesion	17
PDMS pillar with p(DMA-co-MEA-coNIPAAm) coating	Structured surface with coating	Micro-structured surface, polymer synthesis, coating	Covalent bond and hydrogen bonding interactios	60 s	~8, underwater	Thermo-responsiveness	18

Poly(dopamine-co-acrylate)	Polymer solution	Complex polymer synthesis	Covalent bond and hydrogen bonding interaction	15 min	~40, wet	n/a	19
P(VGal-*co*-BA)	Polymer solution	Complex polymer synthesis	Covalent bond, hydrophobic and hydrogen bonding interactions	24 h	~200, wet	n/a	20

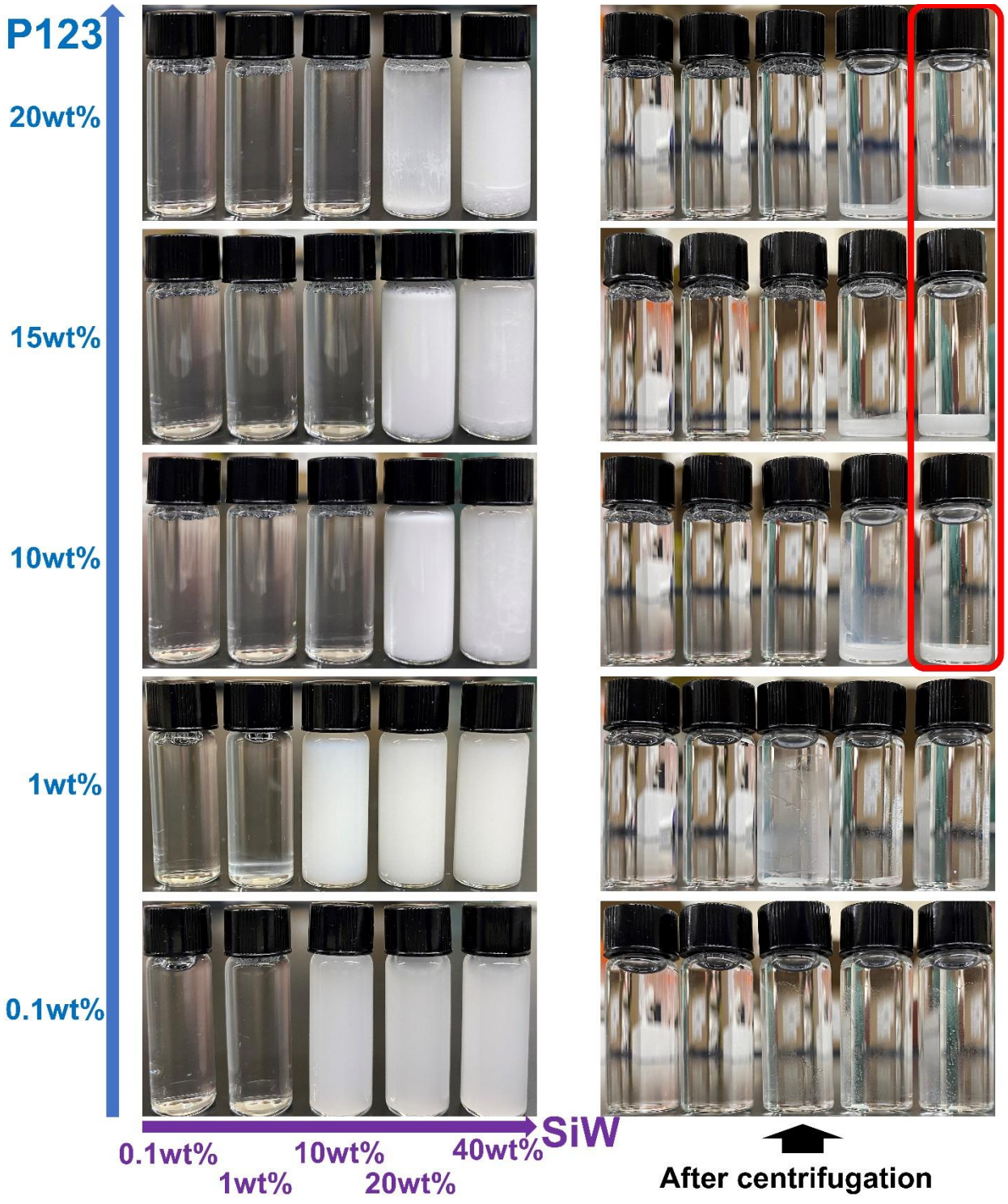

Figure S1. Corresponding pictures of the phase diagram between SiW and P123 with various concentrations. (Left: upon mixing of the two aqueous solutions; Right: after centrifugation)

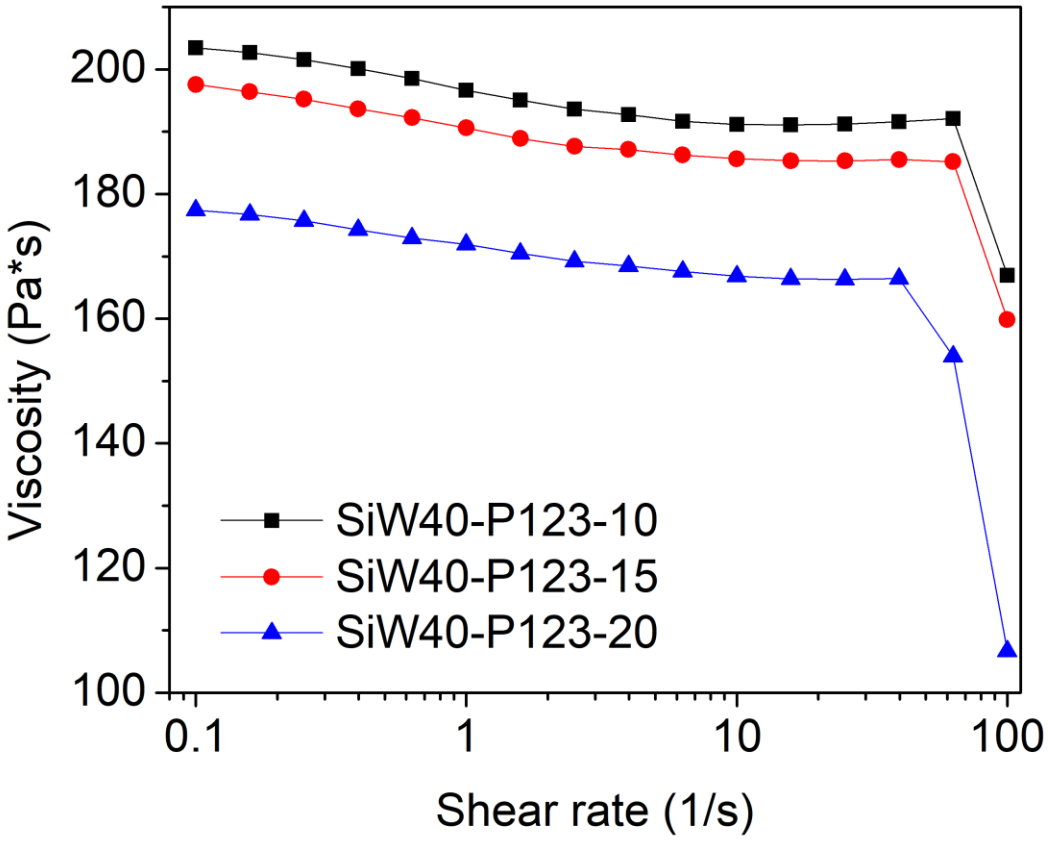

Figure S2. Viscosities of SiW40-P123-10, SiW40-P123-15, SiW40-P123-20 coacervates with shear rate ranging from 0.1 to 100/s.

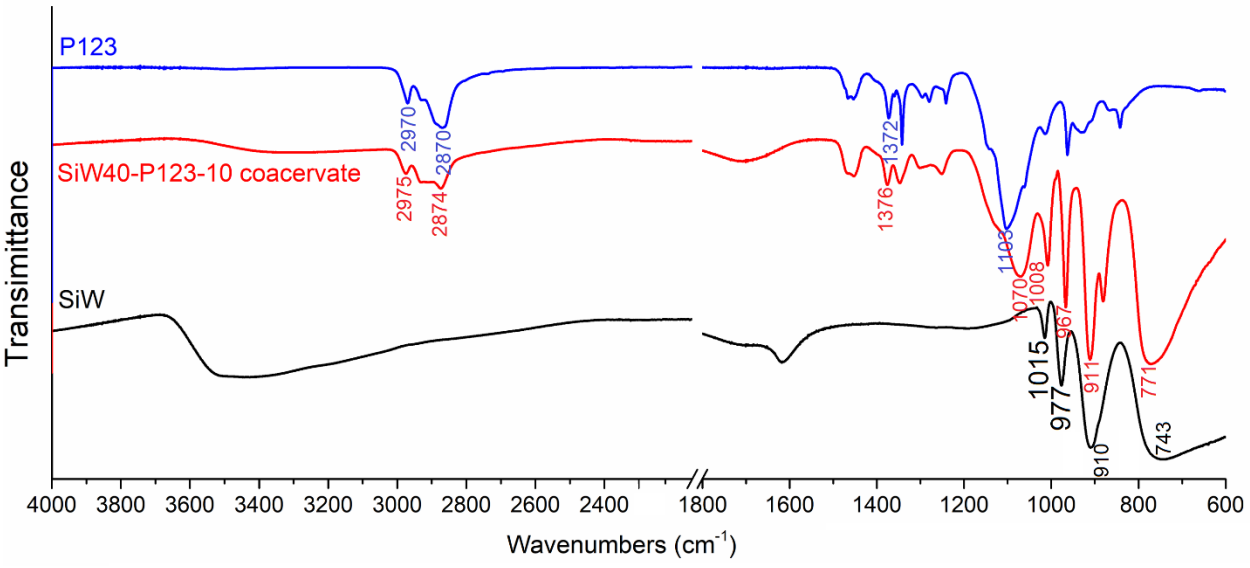

Figure S3. FTIR spectra of P123, SiW and freeze-dried SiW40-P123-10 coacervate.

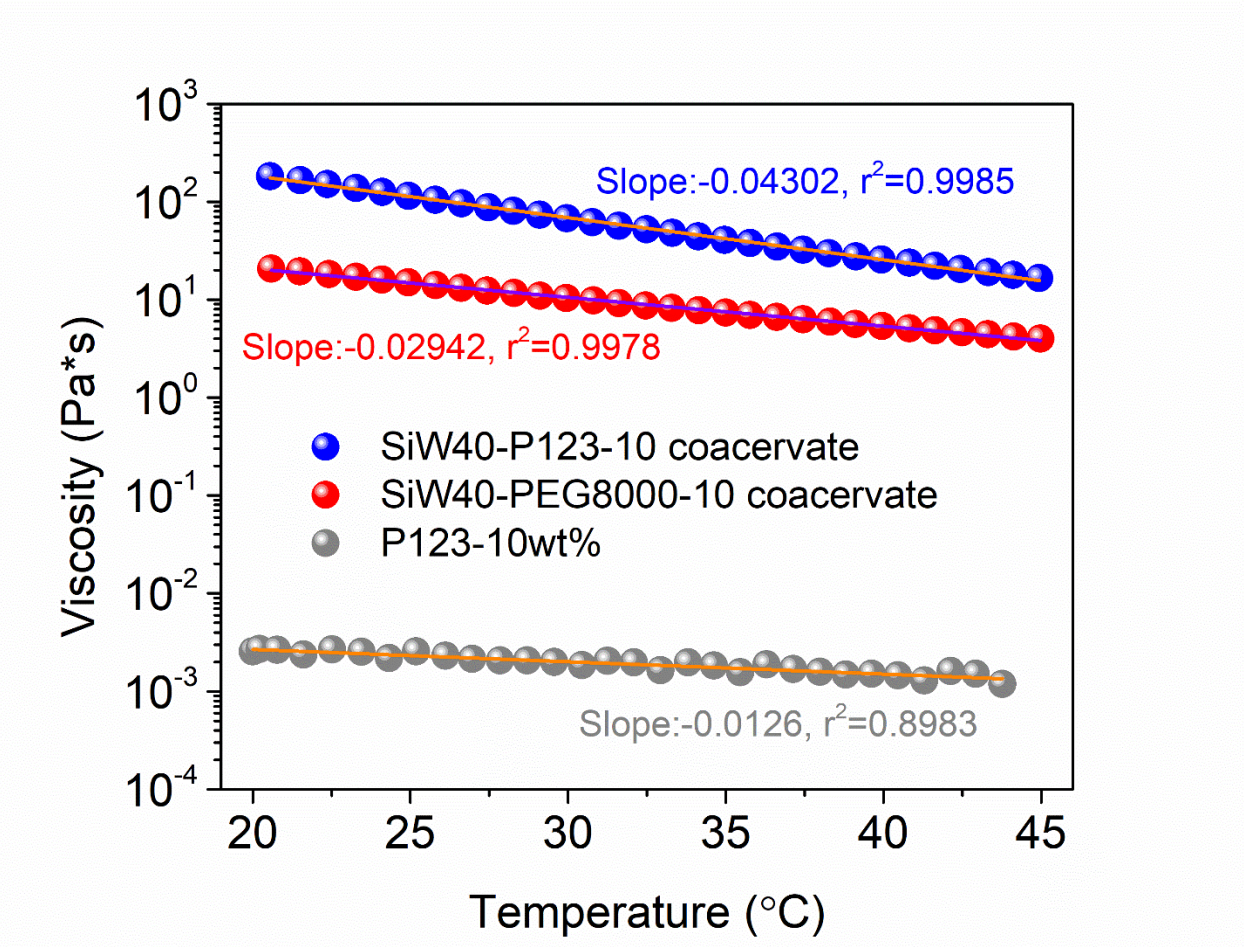

Figure S4. Variations of viscosity versus temperature for SiW40-P123-10 coacervate, SiW40-PEG8000-10 coacervate and 10 wt% P123 aqueous solution.

Figure S5. Pictures for the formation of SiW40-P123-10 coacervate and the corresponding supernatant prepared with SiW solution at pH=1.14 (left) and the mixture of 40 wt% SiW (pH= 1.75) and 10 wt% P123 aqueous solutions (right).

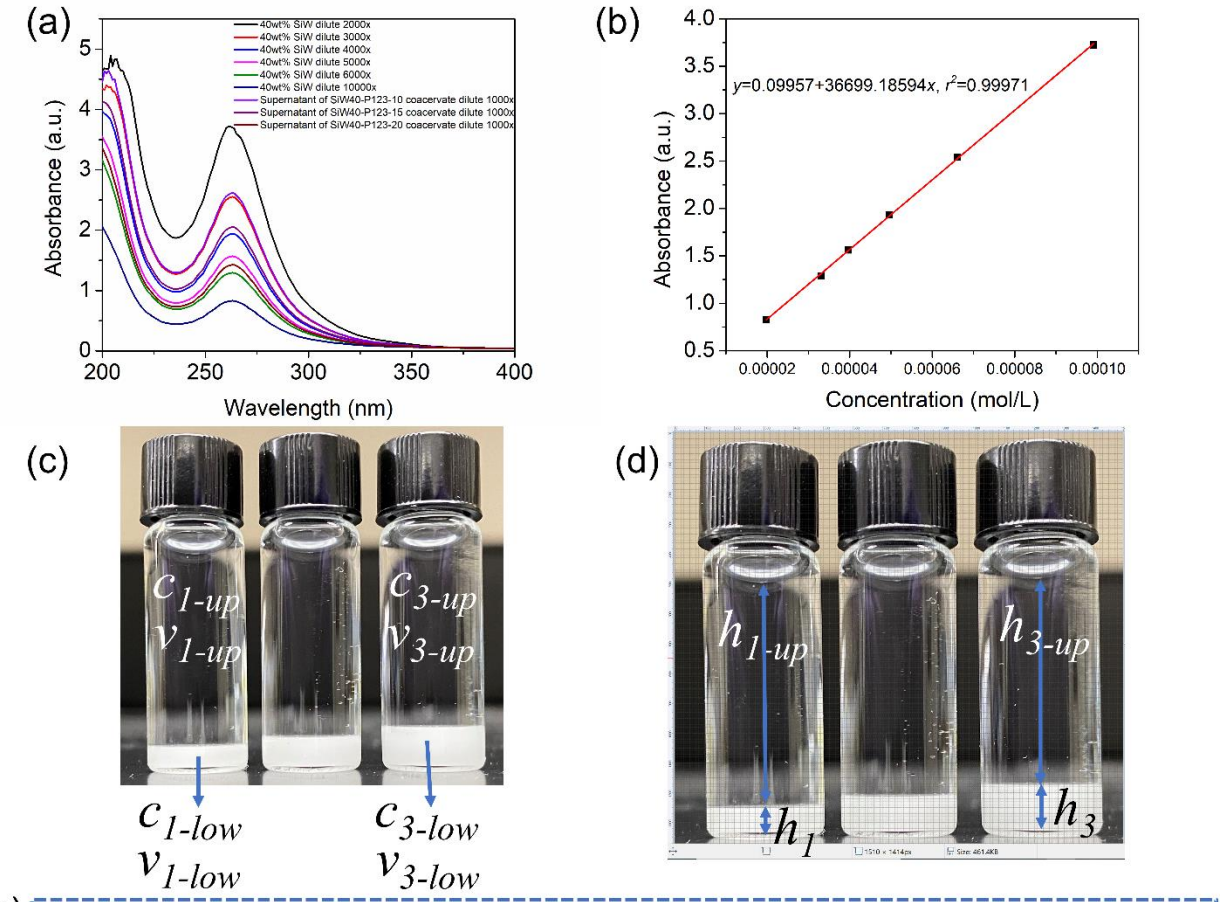

(e)

Mixing 1ml 40wt% SiW and 1ml 10/15/20wt% P123 , respectively.

m(1ml 40wt% SiW)=(1.423g+1.4299g+1.4268g)/3=1.4265g

*c=c(40wt% SiW)=n/v=m/MV=0.4*1.4265g/(2878.17g/mol*1ml)=0.19825mol/l*

h_1*=83 pixels,* $h_{1\text{-}up}$*=756 pixels,* h_3*=156 pixels,* $h_{3\text{-}up}$*=690 pixels*

$v_{1\text{-}up} + v_{1\text{-}low}$ *=2ml,* $v_{1\text{-}up}$*:* $v_{1\text{-}low} = h_{1\text{-}up} : h_1$ *=756:83*

$v_{1\text{-}up}$*=1.80215ml,* $v_{1\text{-}low}$*=0.19785ml*

$v_{3\text{-}up} + v_{3\text{-}low}$ *=2ml,* $v_{3\text{-}up}$*:* $v_{3\text{-}low} = h_{3\text{-}up} : h_3$ *=690:156*

$v_{3\text{-}up}$*=1.63121ml,* $v_{3\text{-}low}$*=0.36879ml*

$v_{3\text{-}low}/v_{1\text{-}low}$*= 0.36879ml/ 0.19785ml=186.4%, increased by 86.4%*

$c_{1\text{-}up}$ *=(y-0.09957)/36699.18594*1000=(2.605-0.09957)/36699.18594*1000=0.06827mol/l*

$c_{3\text{-}up}$ *=(y-0.09957)/36699.18594*1000=(1.419-0.09957)/36699.18594*1000=0.03595mol/l*

$c_{1\text{-}up}\, v_{1\text{-}up} + c_{1\text{-}low}\, v_{1\text{-}low}$ *=c*1ml,* $c_{1\text{-}low}$*=0.38017mol/l*

$c_{3\text{-}up}\, v_{3\text{-}up} + c_{3\text{-}low}\, v_{3\text{-}low}$ *=c*1ml,* $c_{3\text{-}low}$*=0.37856mol/l*

Figure S6. Calculation of volume of SiW-P123 coacervate phases and corresponding supernatants as well as concentration of SiW in SiW-P123 coacervate phases. (a) UV-vis was employed to measure light absorbance of a series of diluted 40wt% SiW aqueous solution and diluted supernatants of SiW40-P123-10/15/20 coacervates. It was demonstrated that SiW has a characterized absorption peak at 262.6nm.[21] (b) Standard absorbance-concentration relationship

was plotted based on results of (a), where concentration of SiW in supernatants of SiW40-P123-10/15/20 coacervates can be calculated according to the fitted linear equation. (c) Representation of concentration of SiW in SiW40-P123-10 ($c_{1\text{-}low}$) and SiW40-P123-20 ($c_{3\text{-}low}$) coacervate phases as well as corresponding supernatants ($c_{1\text{-}up}$ and $c_{3\text{-}up}$). And representation of volumes of SiW40-P123-10 ($v_{1\text{-}low}$) and SiW40-P123-20 ($v_{3\text{-}low}$) coacervate phases as well as volumes of their corresponding supernatants ($v_{1\text{-}up}$ and $v_{3\text{-}up}$). (d) The heights of SiW40-P123-10 (h_1) and SiW40-P123-20 (h_3) coacervate phases and corresponding supernatant phases ($h_{1\text{-}up}$ and $h_{3\text{-}up}$) were measured by counting number of pixels in the vertical direction. (e) The deduction process of calculating volume ratio of SiW40-P123-20 coacervate phase to SiW40-P123-10 coacervate phase as well as concentrations of SiW in their coacervate phases.

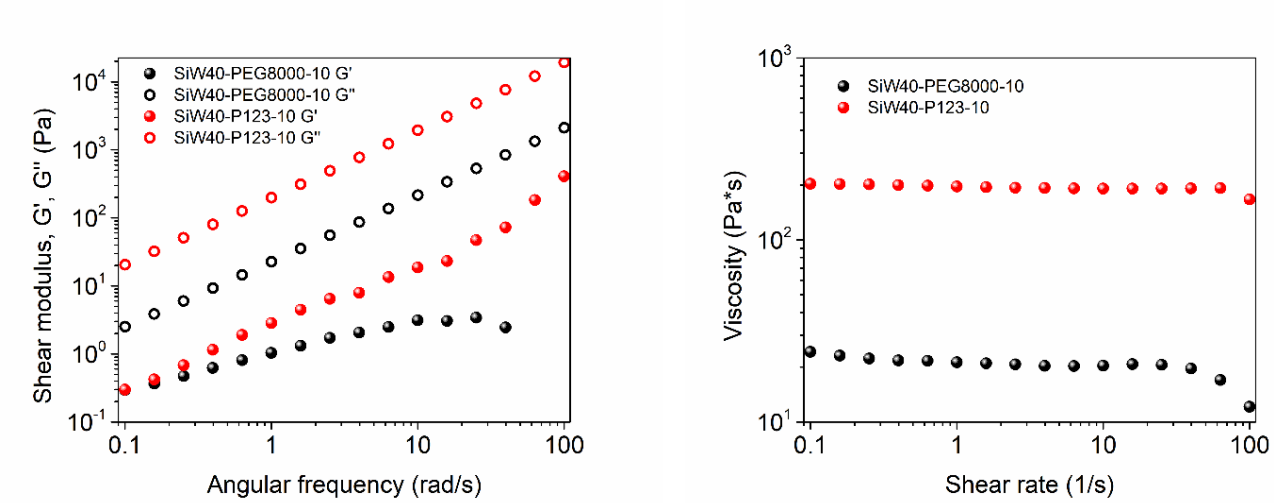

Figure S7. Shear storage modulus, shear loss modulus and viscosity of SiW40-P123-10 coacervate and SiW40-PEG8000-10 coacervate.

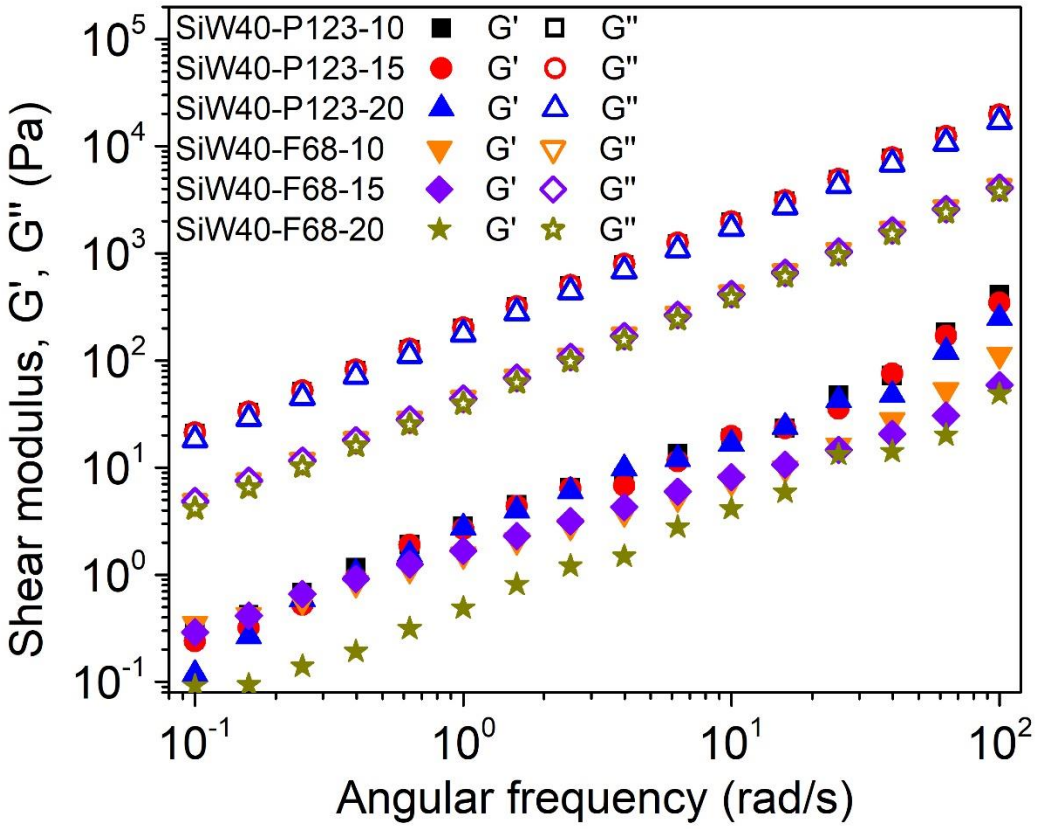

Figure S8. Shear loss modulus G'' and shear storage modulus G' of SiW40-P123-10, SiW40-P123-15, SiW40-P123-20, SiW40-F68-10, SiW40-F68-15, SiW40-F68-20 coacervates.

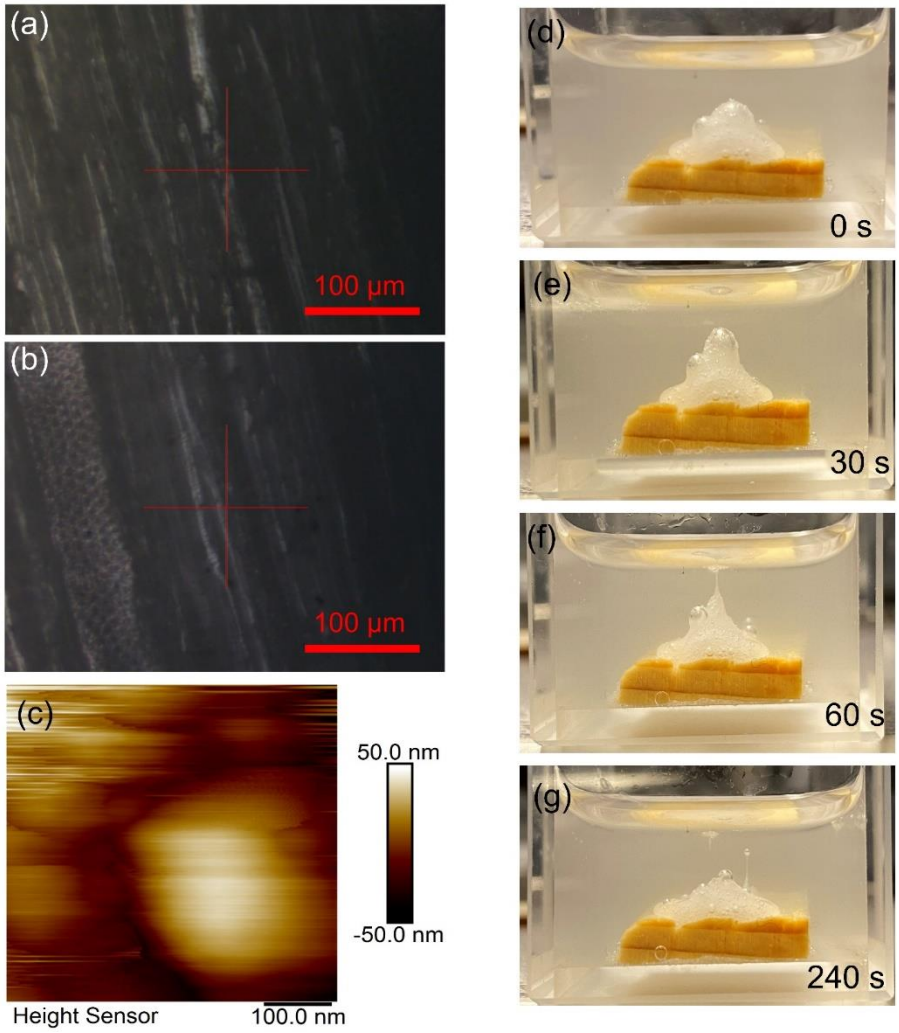

Figure S9. (a-b) Microtubes and micropores on the wood surface observed under an optical microscope coupled with AFM. (c)AFM image of the rough wood surface. (d-g) SiW40-P123-10 coacervate could spread on the wood surface.

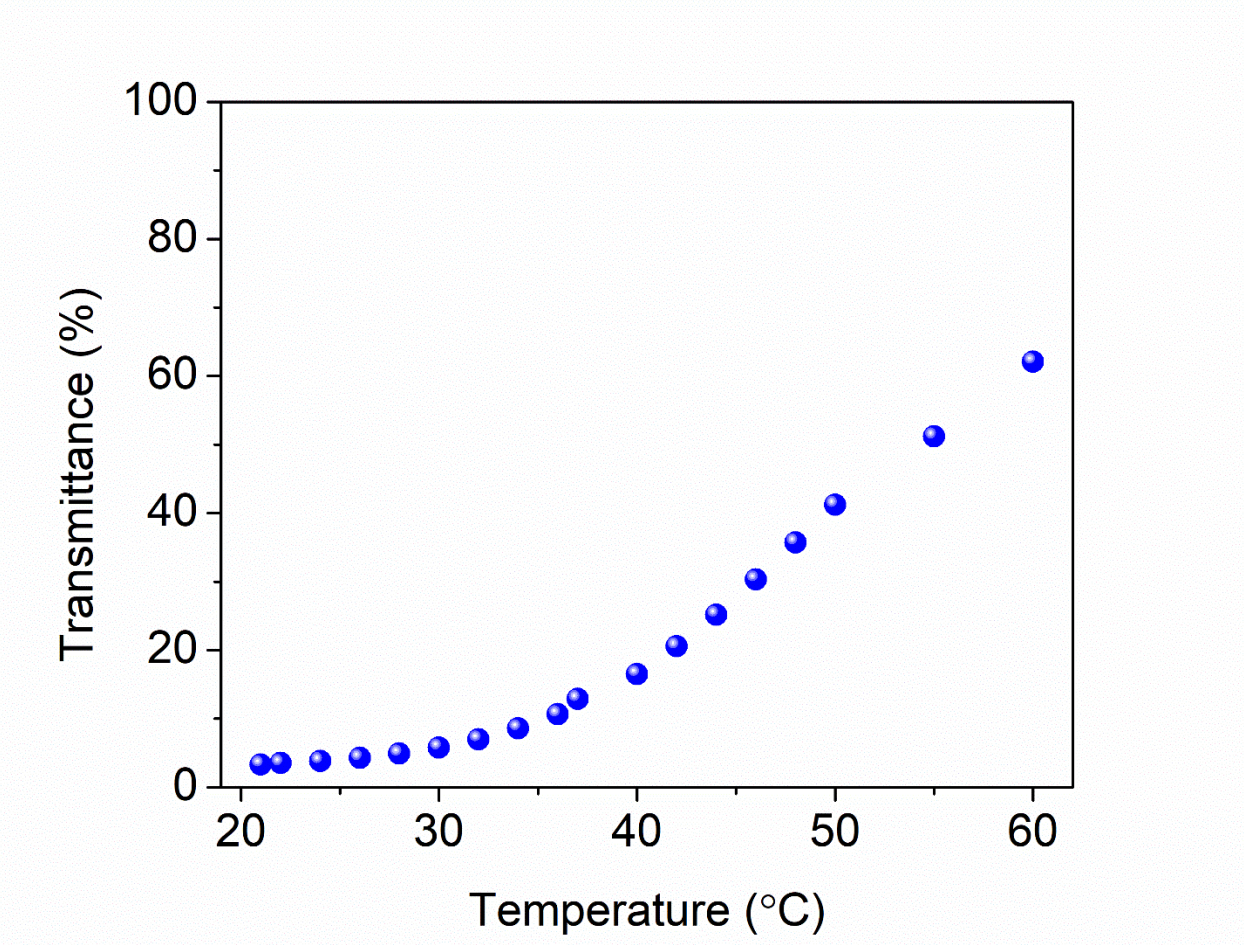

Figure S10. The change of transmittance at 550 nm of the SiW40-P123-10 coacervate with temperature ranging from 21 ℃ to 60 ℃.

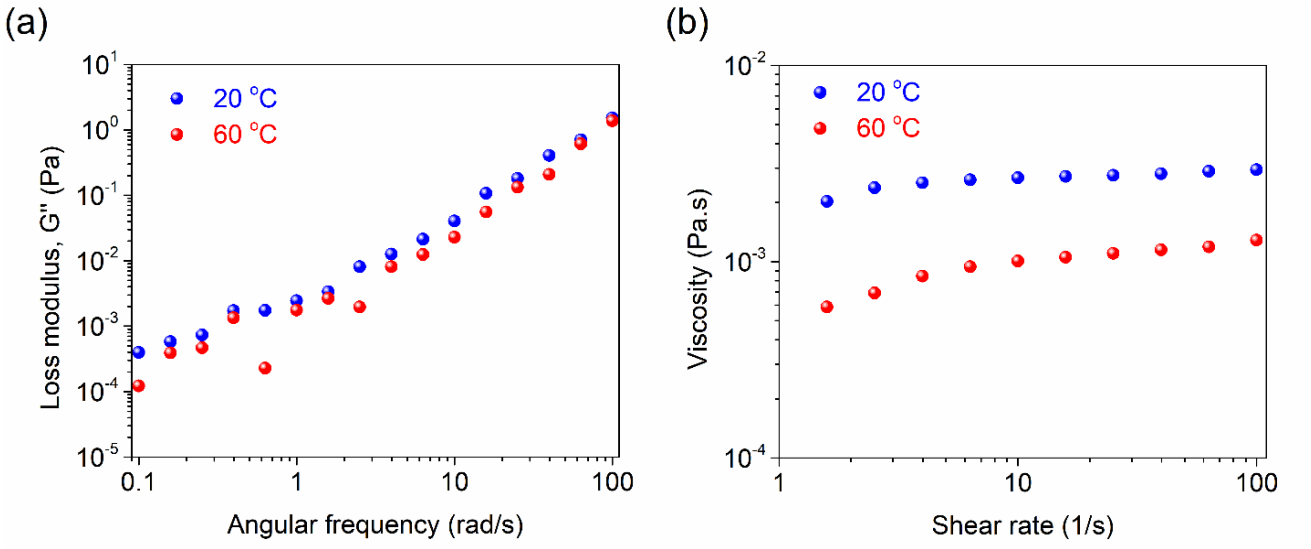

Figure S11. Shear loss modulus and viscosity of P123 aqueous solution at temperatures of 20 ℃ and 60 ℃.

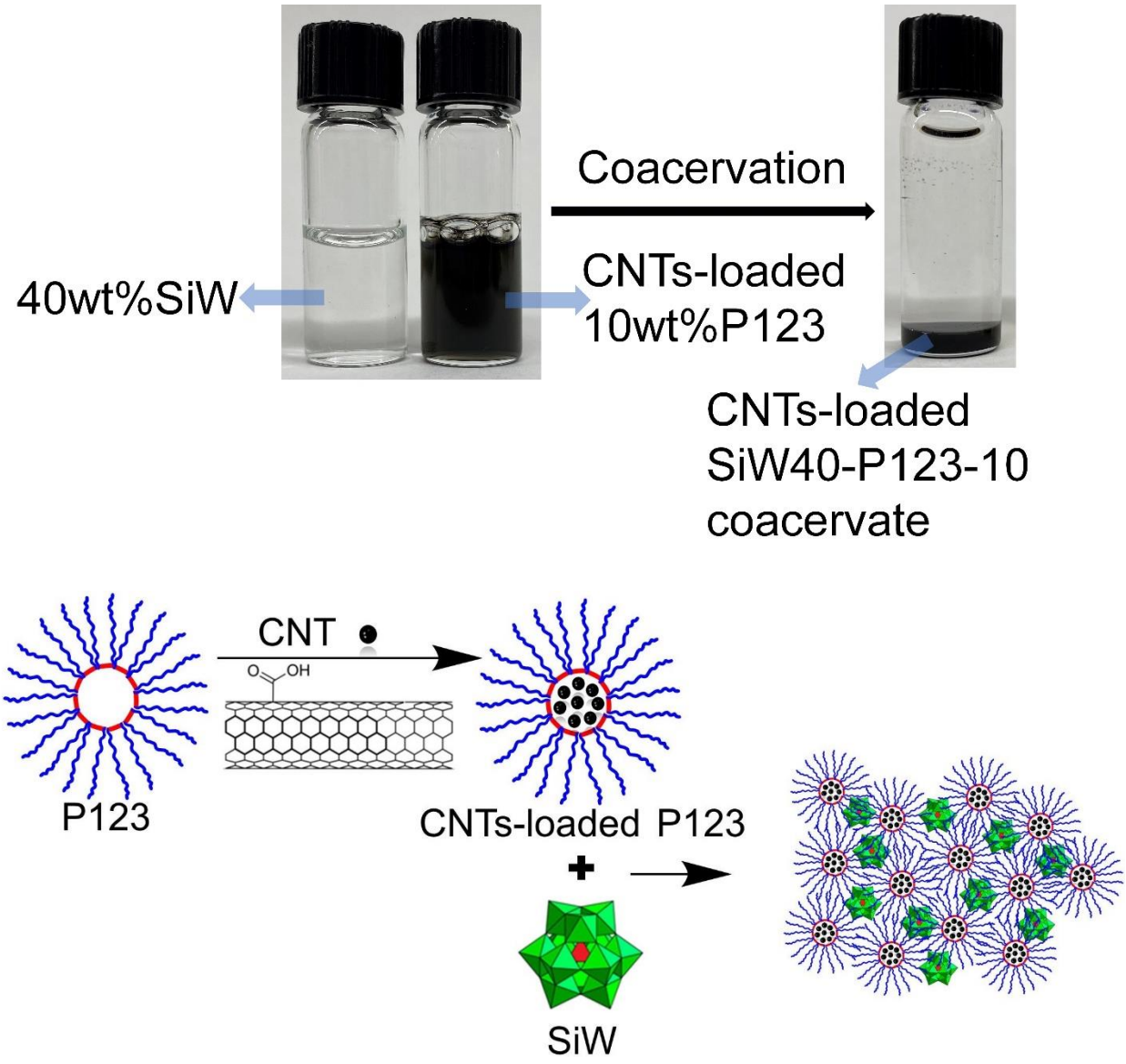

Figure S12. CNTs-loaded SiW40-P123-10 coacervate and corresponding schematic intermolecular interactions.

References

1. Q. Peng, J. Chen, Z. Zeng, T. Wang, L. Xiang, X. Peng, J. Liu and H. Zeng, *Small*, 2020, **16**, 2004132.
2. K. Kim, M. Shin, M.-Y. Koh, J. H. Ryu, M. S. Lee, S. Hong and H. Lee, *Adv. Funct. Mater.*, 2015, **25**, 2402-2410.
3. Z. Wang, S. Zhang, S. Zhao, H. Kang, Z. Wang, C. Xia, Y. Yu and J. Li, *Chem. Eng. J.*, 2021, **404**, 127069.
4. C. Wei, X. Zhu, H. Peng, J. Chen, F. Zhang and Q. Zhao, *ACS Sustainable Chem. Eng.*, 2019, **7**, 4508-4514.
5. D. Lee, H. Hwang, J. S. Kim, J. Park, D. Youn, D. Kim, J. Hahn, M. Seo and H. Lee, *ACS Appl. Mater. Interfaces*, 2020, **12**, 20933-20941.
6. 6 J. Xu, X. Li, J. Li, X. Li, B. Li, Y. Wang, L. Wu and W. Li, *Angew. Chem. Int. Ed.*, 2017, **56**, 8731-8735.
7. A. Narayanan, J. R. Menefee, Q. Liu, A. Dhinojwala and A. Joy, *ACS Nano*, 2020, **14**, 8359-8367.
8. P. G. Lawrence and Y. Lapitsky, *Langmuir*, 2015, **31**, 1564-1574.
9. C. Cui, C. Fan, Y. Wu, M. Xiao, T. Wu, D. Zhang, X. Chen, B. Liu, Z. Xu, B. Qu and W. Liu, *Adv. Mater.*, 2019, **31**, 1905761.
10. H. Fan, J. Wang, Z. Tao, J. Huang, P. Rao, T. Kurokawa and J. P. Gong, *Nat. Commun.*, 2019, **10**, 5127.
11. H. Fan, J. Wang and J. P.Gong, *Adv. Funct. Mater.*, 2020, **31**, 2009334.
12. S. Bai, X. Zhang, P. Cai, X. Huang, Y. Huang, R. Liu, M. Zhang, J. Song, X. Chen and H. Yang, *Nanoscale Horiz.*, 2019, **4**, 1333-1341.

13. C. Cui,; T. Wu, F. Gao, C. Fan, Z. Xu, H. Wang, B. Liu and W. Liu, *Adv. Funct. Mater.*, 2018, **28**, 1804925.
14. A. Li, Y. Jia, S. Sun, Y. Xu, B. B. Minsky, M. A. C. Stuart, H. Cölfen, R. von Klitzing and X. Guo, *ACS Appl. Mater. Interfaces*, 2018, **10**, 10471-10479.
15. X. Liu, Q. Zhang, L. Duan and G. Gao, *Adv. Funct. Mater.*, 2019, **29**, 1900450.
16. X. Li, Z. Du, Z. Song, B. Li, L. Wu, Q. Liu, H. Zhang and W. Li, *Adv. Funct. Mater.*, 2018, **28**, 1800599.
17. Y. Zhao, Y. Wu, L. Wang, M. Zhang, X. Chen, M. Liu, J. Fan, J. Liu, F. Zhou and Z. Wang, *Nat. Commun.*, 2017, **8**, 2218.
18. Y. Ma, S. Ma, Y. Wu, X. Pei, S. N. Gorb, Z. Wang, W. Liu and F. Zhou, *Adv. Mater.*, 2018, *30*, 1801595.
19. H. Zhang, L. P. Bré, T. Zhao, Y. Zheng, B. Newland and W. Wang, *Biomaterials*, 2014, **35**, 711-719.
20. K. Zhan, C. Kim, K. Sung, H. Ejima and N. Yoshie, *Biomacromolecules*, 2017, **18**, 2959-2966.
21. D. Bajuk-Bogdanović, I. Holclajtner-Antunović, M. Todorović, U. B. Mioć and J. Zakrzewska, *J. Serb. Chem. Soc.*, 2008, **73**, 197-209.